Precession of an Electron-Magnetohydrodynamic Field-Reversed Configuration

R. L. Stenzel,* M. C. Griskey, J. M. Urrutia, and K. D. Strohmaier

Department of Physics and Astronomy, University of California, Los Angeles, California 90095-1547

(Received 14 January 2002; published 23 April 2002)

A field-reversed configuration is generated in a large laboratory plasma in the parameter regime of electron magnetohydrodynamics. During its free relaxation, the magnetic moment is observed to precess when tilted from its original axis. The precession velocity is the electron drift velocity in the toroidal current layer. The precession is a manifestation of frozen-in field lines in a moving electron fluid.

DOI: 10.1103/PhysRevLett.88.185004 PACS numbers: 52.30.Cv, 52.55.Hc

The magnetic topology of a field reversed configuration (FRC) can be described by a poloidal field opposite to an externally driven uniform field. The poloidal field is produced by plasma currents and there is no externally driven toroidal magnetic field. Devices with this magnetic topology are of potential interest for confinement of fusion plasmas due to a high beta and absence of toroidal coils [1]. However, magnetohydrodynamic (MHD) theory predicts a destructive tilting instability [2] which has not occurred in many experiments [3–5]. One explanation has been the stabilizing effect of ions with large Larmor radii, i.e., non-MHD effects [6,7]. FRCs have also been observed in the limit of completely unmagnetized ions [8,9], where the theory of electron MHD (EMHD) applies [10]. We describe in this Letter first observations of a precession instability, a property unique to EMHD FRCs. When the FRC field becomes inclined to the uniform field, $\mathbf{B}_0$, its field precesses around its original direction. The precession occurs at the velocity of the drifting electrons associated with toroidal currents, which are a manifestation of frozen-in field lines governed by $\mathbf{E} + \mathbf{v} \times \mathbf{B} = 0$.

This basic-physics experiment is performed in a large, uniform laboratory plasma (Fig. 1) of relatively high density ($n_e \simeq 6 \times 10^{11}$ cm^{-3}, $p_n \simeq 0.3$ mTorr, Ar) and low background magnetic field ($\mathbf{B}_0 \simeq -5\,\mathrm{G}\,\hat{\mathbf{z}}$), where only the electrons are magnetized (Larmor radius $r_{ce} \simeq 1.2$ cm for $kT_e \simeq 3$ eV, and $f_{ci}^{-1} \gg t_{\mathrm{FRC\,decay}} \simeq 20\ \mu$s). Pulsed currents are applied to a Helmholtz coil (30 cm diam), generating a dipolar field opposite to and stronger than the uniform field ($B_H \simeq 25$ G on axis). The current pulse is long enough (50 μs) for the field to diffuse into the plasma, at which time ($t = 0$) it is abruptly ($t_{\mathrm{off}} \simeq 2\ \mu$s) switched off so as to observe the free relaxation of the induced FRC. The fields are essentially all contained within the uniform plasma column (80 cm diam), and there are no stabilizing wall currents induced. The cold ions ($kT_i \simeq 0.1$ eV) do not move significantly during the relaxation of the EMHD FRC, which occurs on a time scale ($\leq 15\ \mu$s) long compared to the whistler transit times along the FRC ($\tau_w = L/v_w \simeq 2\ \mu$s for $L \simeq 30$ cm, $v_w \simeq 15$ cm/μs), but short compared to the classical diffusion time ($\tau = \mu_0 \sigma_\perp L^2 \simeq 500\ \mu$s for $\sigma_\perp \simeq 50\ \Omega^{-1}\,\mathrm{cm}^{-1}$). The time-varying magnetic fields inside the plasma are measured with a triple magnetic probe, recording (B_x, B_y, B_z) at a given position. By repeating the highly reproducible ($\pm 1\%$) discharges and moving the probe to many positions, the vector field $\mathbf{B}(\mathbf{r}, t)$ is obtained with high resolution ($\Delta r \simeq 0.75$ cm, $\Delta t \simeq 10$ ns). Plasma parameters are obtained from a small Langmuir probe ($\pi r^2 \simeq 2.6$ mm^2). The observed precession phenomenon does not start randomly but is also repeatable due to initial conditions which are still under investigation.

The basic field topology is shown in Fig. 2. The direction of the measured magnetic vector field $(B_y, B_z)(0, y, z)$ is shown via unit vectors in Fig. 2a. These unit vectors are tangential to contours of constant poloidal flux, $\Phi = \int B_z 2\pi r\, dr = \mathrm{const}$, shown in Fig. 2b. Thus, poloidal flux contours quantify magnetic field lines provided they are frozen into the electron fluid and there is no reconnection (Fig. 2b). The O-type null points shown in Fig. 2a are centered at the location of the Helmholtz coil. The three-dimensional (3D) null points are located at the intersection of the separatrix ($\Phi = 0$) with the z axis.

The motion of the flux contours, i.e., field lines, in time is indicated in three snapshots in Figs. 3a–3c. After switch-off of the coil current, the FRC is maintained by induced toroidal plasma currents. These are predominantly electron Hall currents driven by radial space-charge electric fields, except in the magnetic null region (neutral sheet), where J_θ is directly driven by the inductive

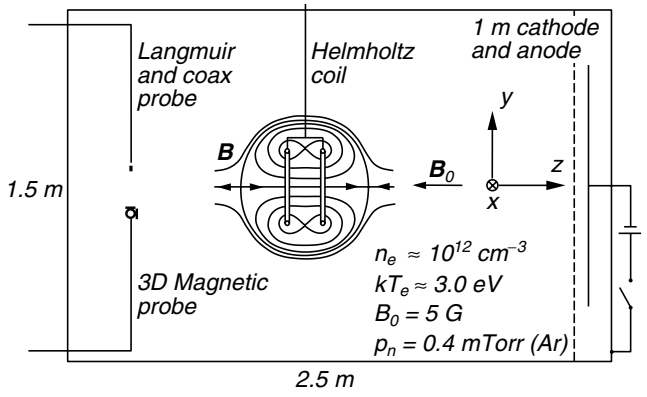

FIG. 1. Experimental setup with basic plasma parameters.

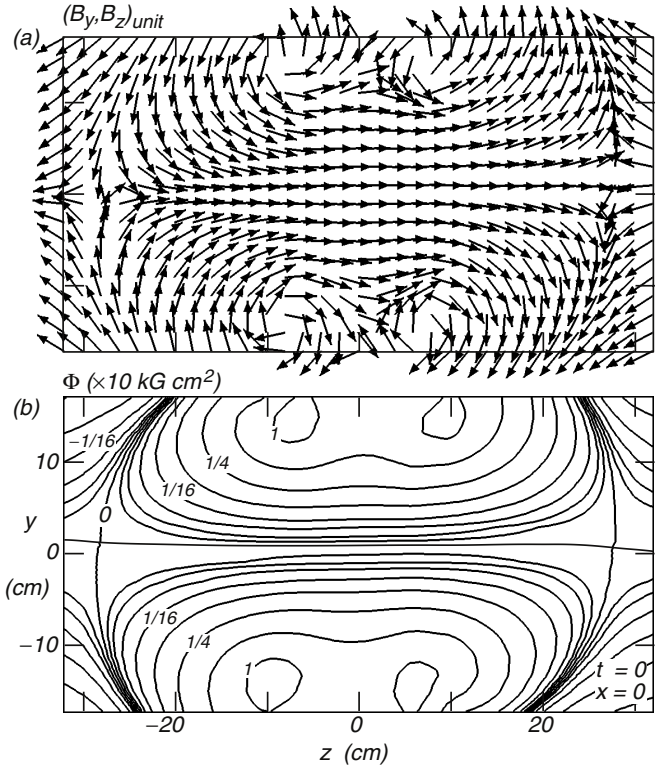

FIG. 2. (a) Measured unit vector field of (B_y, B_z) at switch-off of the coil current ($t = 0$). (b) Calculated contours of constant poloidal flux, $\Phi = \int B_z 2\pi r\, dr = \text{const}$, representing magnetic field lines in ideal fluids.

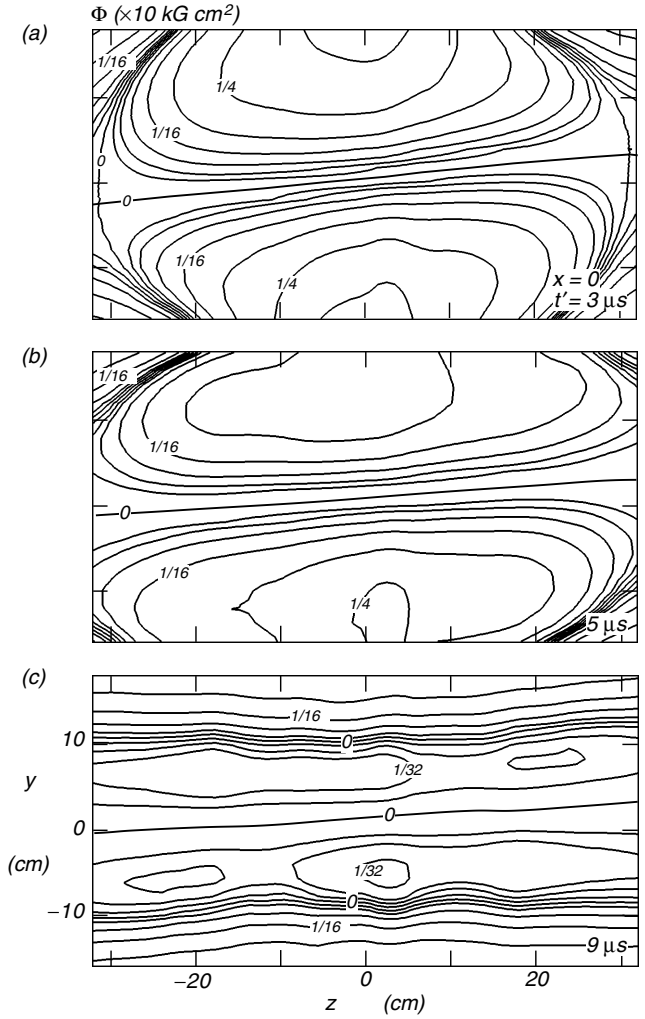

FIG. 3. Magnetic field lines ($\Phi = \text{const}$) of a freely relaxing FRC showing a tilt in the y-z plane which recovers in time.

electric field, $E_\theta \propto -\partial B_z/\partial t$. A characteristic quantity of an FRC is its ellipticity, $\varepsilon = l_s/2r_s$, where l_s is the axial distance between the cusp null points and r_s is the radius of the separatrix at $z = 0$. Another characteristic number is s_e, the distance between the magnetic null layer and the separatrix, normalized to the electron Larmor radius in the external field. In our experiment, $\varepsilon = 1.06$ and $s_e \simeq (r_s - r_0)/r_{ce} \simeq 17.6\ \text{cm}/1.2\ \text{cm} = 14.6$, which yields a stability parameter of $s_e/\varepsilon \simeq 13.8$. In MHD theory, where s is based on the ion Larmor radius, the FRC would be highly unstable to tilting [11]. If the EMHD FRC is also stabilized by large electron Larmor effects, one would expect to observe strong tilting. During the free relaxation, the ellipticity of the EMHD FRC increases, the flux decreases, and the stability parameter becomes $s_e/\varepsilon \simeq 5/2.03 = 2.46$ at $t \simeq 10\ \mu$s. Toward the end of the FRC's lifetime ($t \approx 15\ \mu$s), both the ellipticity and s_e decrease such that $s_e/\varepsilon \simeq 1.35$ at $t \simeq 13\ \mu$s (not shown in Fig. 3).

The dynamics of the freely relaxing FRC is largely governed by electron flows. The toroidal current produces an electron drift, $v_d = -J_\theta/ne$, which rotates the highly frozen-in field lines in the θ direction within the FRC, but not much beyond the separatrix. Thus, there is a twist of the field lines near each end of the FRC, but none in the center. No net helicity is produced since the twists cancel. The twists (i.e., $\pm B_\theta$ components) at the ends of the FRC imply axial currents, which close in poloidal loops. The associated electron flow across the separatrix carries the field lines axially outward, leading to the observed elongation of the FRC. The 3D null points are improper spiral nulls [8,12]. The null points prevent the field convection in the whistler mode, which characterizes the field dynamics at small amplitudes ($B_H < B_0$) [13].

The poloidal flux decreases during the relaxation. By observing the motion of field lines ($\Phi = \text{const}$ contours), one finds that no field lines pass through the 3D null points on axis. Instead, they all move toward the elongated neutral sheet, tear into small islands, and vanish. Thus the closed field lines never cross the separatrix but are annihilated in the two-dimensional neutral sheet. Magnetic energy is converted into electron thermal energy in the current sheet, but not at the cusps.

During the decay, the FRC field exhibits a small inclination (see Fig. 3b) but recovers and remains on the average aligned with $\mathbf{B}_0$. In order to describe the inclination in time, we present a stereoscopic display in Fig. 4 of a hodogram representation of the magnetic dipole moment, $\mathbf{m} = \frac{1}{2}\int \mathbf{r} \times \mathbf{J}\, dV$, where $\mathbf{J} = \nabla \times \mathbf{B}/\mu_0$ and $\mathbf{r}$ is the

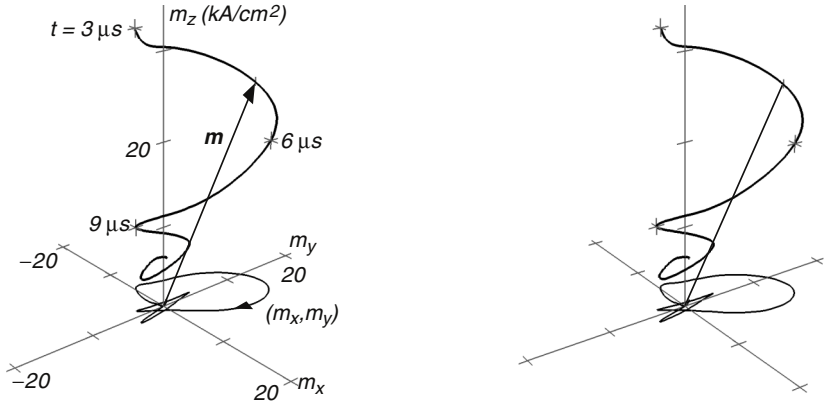

FIG. 4. Hodogram of the magnetic moment, $\mathbf{m} = \frac{1}{2}\int \mathbf{r} \times \mathbf{J}\, dV$. The vector $\mathbf{m}$ can be viewed stereoscopically by placing an opaque divider vertically between the images so as to see the right/left image with the right/left eye only. The vector $\mathbf{m}$ rotates around the z axis ($\| -\mathbf{B}_0$), while decaying in magnitude. From the projection (m_x, m_y), one finds the precession velocity, which coincides with the toroidal electron drift.

radius vector from the symmetry axis. This approach is more accurate than judging the field inclination from the centers of the O points which are not the only locations of large currents. (To view it in 3D, it helps to place an opaque divider between the images so that the left/right eye can see only the left/right figure. Alternatively, the authors suggest that an inexpensive viewer, such as the Stereopticon 707 [14], be employed.) During the free relaxation ($3 \lesssim t \lesssim 15$ μs), the magnetic moment rotates around the z axis ($\| -\mathbf{B}_0$), while decreasing in magnitude. A projection of $\mathbf{m}$ onto the x-y plane ($z = 0$) shows that the precession period of the major rotation is $T_p \simeq 5$ μs, and the direction is right handed, which corresponds to the toroidal electron drift direction.

A tilt of $\mathbf{m}$ implies that the toroidal current layer is no longer symmetric around the z axis. In addition to the toroidal current there is an axial current component J_z. This current is found from the measured fields ($\mu_0 J_z = \partial B_y/\partial x - \partial B_x/\partial y$) and displayed in Fig. 5 at four different times in the x-y plane. There are two opposing axial currents where the inclined current cylinder intersects the x-y plane. In time, the current distribution rotates, hence its magnetic moment (m_x, m_y, see arrow) rotates as earlier shown in Fig. 4. The profile of the toroidal current component J_θ is an annulus of diameter equal to the spacing of $|J_{z,\max}|$.

The velocity of the rotation is close to the toroidal electron drift velocity, $v_d = -J_\theta/ne \simeq 8 \times 10^6$ cm/s for $J_\theta \simeq 0.8$ A/cm^2, $n \simeq 6 \times 10^{11}$ cm^{-3}. Figure 6 shows the electron drift velocity and the rotation velocity of $\mathbf{m}$ at the radius of the current layer in time. It is interesting to note that, as the radius of the current layer shrinks, the current density does not significantly change throughout the relaxation of the FRC. The current density during the free relaxation neither varies significantly with different initial values of B_H, indicating a current-limiting

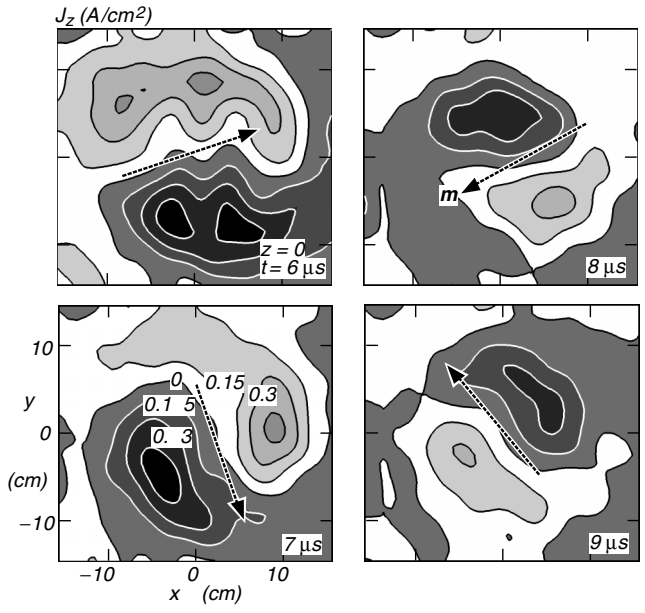

FIG. 5. Axial current density, $J_z(x, y, 0)$, at four consecutive time steps showing a rotation of its dipole moment.

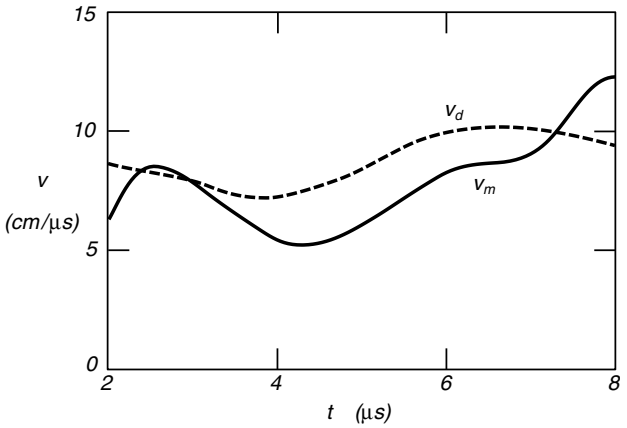

FIG. 6. Electron drift velocity, v_d, and velocity of the rotating magnetic field, v_m, in the toroidal current layer. Both are comparable and do not change significantly during the decay of the FRC.

process controls the decay. The self-consistent electric field in the neutral layer is close to the Dreicer field [15] ($E_\theta \simeq E_D = m\nu_{ei}v_{th}/e \simeq 0.2$ V/cm), but no runaway electron distributions are found in the current sheet. However, strong current-driven ion sound turbulence is observed in the neutral sheet [$\delta n/n \approx 5\%$; note $v_d \simeq 30(kT_e/m_i)^{1/2}$, $T_e \simeq 10T_i$], which can produce anomalous collisions [$\nu^* \approx \omega_{pe}(\delta n/n)^2 \approx 10^8\ s^{-1}$] [16] and explain the observed low ratio $J_\theta/E_\theta \simeq 5\ \Omega^{-1}\,cm^{-1} \simeq 0.1\sigma_{Spitzer}$ for $kT_e \simeq 3$ eV. The electron temperature increases during the FRC relaxation ($kT_e = 2 \rightarrow 4$ eV), which accounts for the loss of magnetic energy.

We now offer an explanation for the precession in terms of electron fluid flows and the frozen-in concept: The current density of a slightly inclined current layer can be decomposed into toroidal and axial components. The axial current forms a line dipole (Fig. 5), whose magnetic field is perpendicular to the toroidal electron flow. The frozen-in field lines are convected in the direction and with the speed of the rotating fluid, as observed. Superposition of the rotating field components (B_x, B_y) and the poloidal field B_z leads to the precessing of the field.

It is interesting to speculate that if a transverse synchronously rotating magnetic field was externally applied, the precessing current layer could be maintained. This concept differs from the conventional mechanism for rf current-driven FRCs [17,18] or rotamaks [19], where nonlinear effects produce the toroidal current and maintain the FRC.

In summary, a new phenomenon, the precession instability of an EMHD FRC, has been observed and explained. It is a unique feature of the EMHD regime that an initial tilt turns into a precession due to the rotating electron fluid. In MHD, a toroidal current does not imply a rotating fluid; hence the tilt grows without precessing.

The authors gratefully acknowledge support for this work from NSF Grant No. PHY 0076065.

*Electronic addresses: http://www.physics.ucla.edu/plasma-exp/; stenzel@physics.ucla.edu

[1] V. I. Khvesyuk, S. V. Ryzhkov, J. F. Santarius, G. A. Emmert, C. N. Nguyen, and L. C. Steinhauer, Fusion Technol. **39**, No. 1T, 410–413 (2001).
[2] M. N. Rosenbluth and M. N. Bussac, Nucl. Fusion **19**, 489 (1979).
[3] M. Tuszewski, Nucl. Fusion **28**, 2033 (1988).
[4] J. T. Slough, A. L. Hoffman, R. D. Milroy, R. Maqueda, and L. C. Steinhauer, Phys. Plasmas **2**, 2286 (1995).
[5] Y. Ono and M. Inomoto, Phys. Plasmas **7**, 1863 (2000).
[6] E. V. Belova, S. C. Jardin, H. Ji, and R. Kulsrud, Phys. Plasmas **7**, 4996 (2000).
[7] Y. A. Omelchenko, Phys. Plasmas **7**, 1443 (2000).
[8] R. L. Stenzel, J. M. Urrutia, M. C. Griskey, and K. D. Strohmaier, Earth Planets Space **53**, 553 (2001).
[9] R. L. Stenzel, J. M. Urrutia, M. C. Griskey, and K. D. Strohmaier, Phys. Plasmas **9**, 1925 (2002).
[10] A. S. Kingsep, K. V. Chukbar, and V. V. Yan'kov, in *Reviews of Plasma Physics* (Consultants Bureau, New York, 1990), Vol. 16, p. 243.
[11] M. Tuszewski, D. C. Barnes, R. E. Chrien, J. W. Cobb, D. J. Rej, R. E. Siemon, D. P. Taggart, and B. L. Wright, Phys. Rev. Lett. **66**, 711 (1991).
[12] C. E. Parnell, J. M. Smith, T. Neukirch, and E. R. Priest, Phys. Plasmas **3**, 759 (1996).
[13] J. M. Urrutia, R. L. Stenzel, and M. C. Griskey, Phys. Plasmas **7**, 519 (2000).
[14] Stereopticon 707, Taylor-Merchant Corp., 211-54 45th Drive, Bayside, NY 11361, U.S.: 1-800-223-6694, non-U.S.: 1-718-224-6661, URL http://www.stereopticon.com/.
[15] H. Dreicer, Phys. Rev. **115**, 238 (1959).
[16] *NRL Plasma Formulary,* edited by J. D. Huba (Naval Research Laboratory, Washington, 1990), p. 29, NRL Publication No. 6790-98-358.
[17] W. N. Hugrass and M. Ohnishi, Plasma Phys. Controlled Fusion **41**, 955 (1999).
[18] A. L. Hoffman, Nuclear Fusion **40**, 1523 (2000).
[19] I. R. Jones, Phys. Plasmas **6**, 1950 (1999).